# A Measurement of the Angular Distribution of Cosmic Muons

**Jennifer Blanchard**

Supervisor: Prof. Francois Corriveau

**Abstract**

Under the supervision of Prof. Francois Corriveau, the spark chamber built at McGill University 16 years ago is refurbished so that the university once again has a working spark chamber. The chamber is used to analyze the trajectory of cosmic muons arriving at the surface of the Earth. A new data acquisition system is developed, consisting of capturing and recording on video the particles' trajectories as they pass through the detector. As well, a new data analysis technique is developed that analyzes each frame of the video and reconstructs the trajectory of the particles to determine the angle of incidence of each particle. Finally, the angular distribution of cosmic rays passing through the detector is measured and compared to currently accepted models. Besides being used as a particle detector in experiments at McGill, the spark chamber is also a great demonstration for public events where it may be shown to fellow students and visitors to the university.

PHYS 479
Research Project Final Report
McGill University

August 24, 2012

# Contents



# 1 Introduction

A spark chamber is an ionization detector used to detect electrically charged particles. In this case, it is used to detect the passage of cosmic muons; particles whose origins are in outer space. In the early 1970's, spark chambers were widely used in particle physics research. Compared to other detectors of the time, spark chambers were less costly and had good spatial and time resolutions, making them the favorable detectors for particle physics research. The spark chamber was later replaced by higher time and spatial resolution detectors in the 1980's and is now used mostly for demonstrations, where it retains the advantage of being a relatively cheap detector to build and directly shows the physical path of the particle.

A discharge between parallel plates was first observed in 1949 by J. Warren Keuffel, who realized that the discharge occurred along the trajectory of the charged particle as it passed through the detector[1]. In its basic form, a spark chamber is simply a stack of parallel metal plates, with every other plate charged to a high voltage (on the order of thousands of volts). The plates are placed in a transparent casing, which is then filled with gas, traditionally a noble gas. As a charged particle traverses the detector, it leaves behind a trail of ionized gas. When the high voltage is applied across the plates, a discharge occurs at the locations of the ionized gas, creating a spark and thus directly showing the location at which the particle traversed the detector.

The spark chamber at McGill University was first built in the summer of 1996 by Anne-Elisabeth Granier and Pascale Sevigny under the supervision of Professor F. Corriveau. It was used for several

years following its construction, but has since been left unused. In particular, an acoustic data acquisition system was developed, but this method remains to be completed.

The main goals of this project are to refurbish the spark chamber for the purpose of measuring certain properties of cosmic muons. In particular, this means measuring the angular distribution of cosmic rays passing through the detector. To do this, a new data acquisition system is developed, as well as new data analysis software. Refurbishing the detector means disassembling, cleaning and reassembling the chamber, as well as replacing the gas within the encasing. With the chamber in working order, the next step is to assemble the electronics, including power supplies, and calibrate the equipment.

Besides measuring the distribution of cosmic muons, the detector may also be used during public events to show visitors to the University and fellow students the passing of cosmic muons directly. It is not only an interesting demonstration, but is also a very relevant and educational experience since these particles pass through us all the time, we just can't see them.

# 2 Theory

## 2.1 Cosmic Rays

Cosmic rays are energetic particles originating in outer space, which some believe to have extragalactic origins. There are two types of cosmic rays: primary and secondary. The primary cosmic rays are composed of $90\%$ protons, while secondary cosmic rays are created when the primary rays enter the atmosphere and collide with air molecules, where particle showers occur. The protons scatter in the atmosphere and produce pions ($\pi^+, \pi^-, \pi^0$) and kaons ($k^+, k^-, k^0$). The charged pions ($\pi^+, \pi^-$) then decay into muons and neutrinos (see figure 1). The muons produced have enough energy to reach the Earth's surface and even penetrate the surface in most cases.

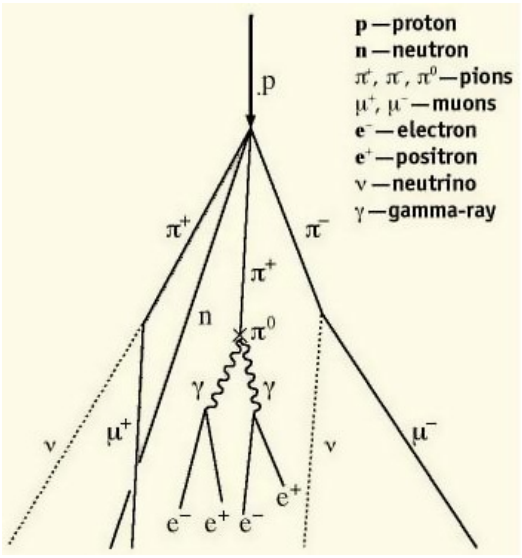


Figure 1: Particle shower in the upper atmosphere. When cosmic rays enter the Earth's atmosphere, they interact with air molecules, resulting in proton scattering. The protons scatter into pions, which then decay into muons.[2]

Although the lifetime of a muon is as short as $2.2\mu s$, muons still manage to reach the Earth's surface

due to the fact that they travel near the speed of light and experience relativistic effects.[3]

### 2.2 Angular Distribution of Cosmic Muons

Of the particles that reach the Earth's surface after passing through the atmosphere, muons are the most abundant of the charged particles. Most are produced in the upper atmosphere and lose approximately $2GeV$ in their descent due to ionization.[4] For this reason, and for the reason that they are charged particles, muons are of particular interest since they are relatively easy to detect. The measurement of the angular distribution of cosmic muons is useful since it may provide information about the sources of cosmic muons.

According to experiment, the overall angular distribution of muons at sea level is approximately $I_0 cos^2\phi$, where $\phi$ is the zenith angle and $I_0 \approx 70$ m$^{-2}$s$^{-1}$sr$^{-1}$ is the flux at $\theta = 0$.[5] The final goal of this project is to verify the $cos^2\phi$ distribution of cosmic rays arriving at the surface of the Earth.

## 3 Experimental Setup

The spark chamber itself (see Appendix A, figure 14) consists of 26 parallel metal plates, placed approximately 1 cm apart. These are placed specifically so that they are exactly parallel, held apart by equally sized rubber stubs and held down by a weight to prevent the plates from warping upwards at the center. These plates are connected to either a large voltage on the order of 12,000 volts or to ground, in an alternating fashion. The plates are enclosed in a tank made of Plexiglas that is filled with helium gas (99.999% pure). Helium is chosen because it ionizes easily and is relatively cheap when compared to other easily ionized gases.

The encasing not only serves to keep in the gas, but also serves to keep out dust, which is an important part of the cleaning process. Any dust that remains on the metal plates will result in a discharge occurring at that location at all times instead of at the location of the particle's passage, resulting in unwanted noise.

Continuously applying a voltage across the plates results in noise due to accumulation of charge on the plates, as well as potentially causing the metal plates to warp. In 1957, T.E. Cranshaw and J.F. De Beer introduced the idea of applying the high voltage to the plates immediately after the passage of the particle and leaving it off at all other times. They also developed the triggering system to do so.[6]

The trigger in this detector is achieved by reading the signal output by two scintillators (figure 15), making sure a muon passes through both (and thus through the detector). There are two scintillating arms (one on top of the chamber, the other on the bottom), which are composed of plastic scintillating materials that emit photons when charged particles pass through. The photons travel along a waveguide until they reach a photomultiplier tube (PMT), powered by a LeCroy power supply, that amplifies and converts the photons into an electrical signal. This signal is then passed to the electronics. (See figure 2 for a schematic diagram of the spark chamber).

The electronics (figure 17) consist of a discriminator that sets a threshold on the signal to reduce background noise, as well as the width of the output signal. The threshold is set to approximately 50mV

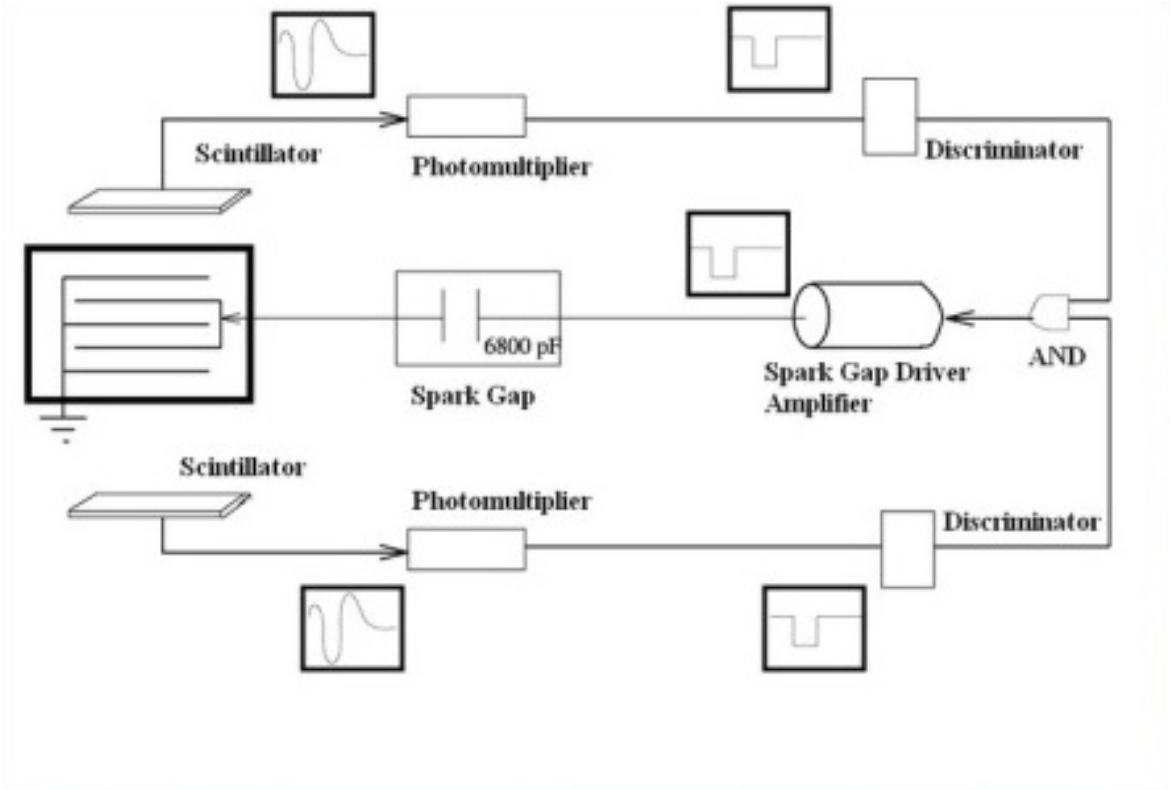


Figure 2: Schematic diagram of the spark chamber and the corresponding electronics system.[7]

and the width to 30 ns. These values have been optimized by a previous student working on the spark chamber.[8] This signal is output by both photomultiplier tubes and sent into the logic unit: an AND gate that outputs a logical 1 if it detects a signal from both PMTs simultaneously. This logical 1 signifies the passing of a charged particle through both of the scintillating arms, and the detector. The logical 1 is amplified and sent to the spark gap, which is itself connected to a high voltage power supply (approximately 12000 volts). When a signal passes through, the spark gap is triggered and the high voltage is applied to the plates in the spark chamber. The accumulation of charge on the plates due to the large voltage discharges at the location of the ionized gas, therefore marking the location at which the particle passed the plates. Immediately after the high voltage is applied, a smaller (100 volts) clearing field is applied across the plates.

The time delay between a particle passing through the chamber and the application of the high voltage on the metal plates is on the order of nano-seconds, while the collection of the ionization charge of the helium between the plates is on the oder of micro-seconds. Therefore, the helium is still ionized when the voltage is applied across the plates.

Since the metal plates in the chamber are charged when a particle is detected and not kept at high voltages at all times, the efficiency of the chamber is reduced. It takes a certain amount of time to charge the spark gap (on the order of milliseconds), so if a particle passes after the voltage has been applied but too soon for the spark gap to recharge, the particle will be missed.

For more images of the detector and it's components, see Appendix A.

## 4 Data Acquisition System

The data acquisition system consists of capturing images of the sparks throughout the chamber to measure the angle of incidence of the particle from these images. This technique is new to the spark chamber at McGill. Several methods were attempted, but some proved to me more difficult than others. Originally, an attempt to capture images with a 30 second exposure was made, so that the resulting image is that of several sparks. (See figures 3 and 4)

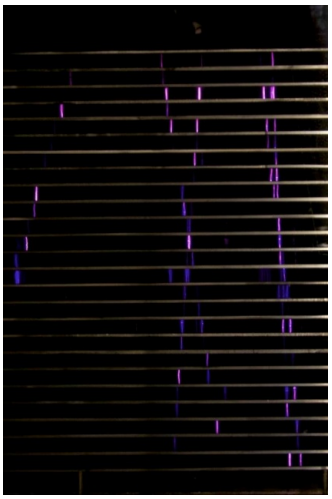

Figure 3: A 30 second exposure of the spark chamber as cosmic muons pass through the detector. The purple and blue sparks show the location at which the helium was ionized when the charged particle passed through. A total of 4 (or 5) trajectories may be observed. The horizontal lines show the metal plates of the detector. Note that this image was taken during a demonstration night at McGill to show sparks in the chamber and is not aligned as it would be during real data collection (where much care is taken to ensure that the camera is perfectly aligned with the detector).

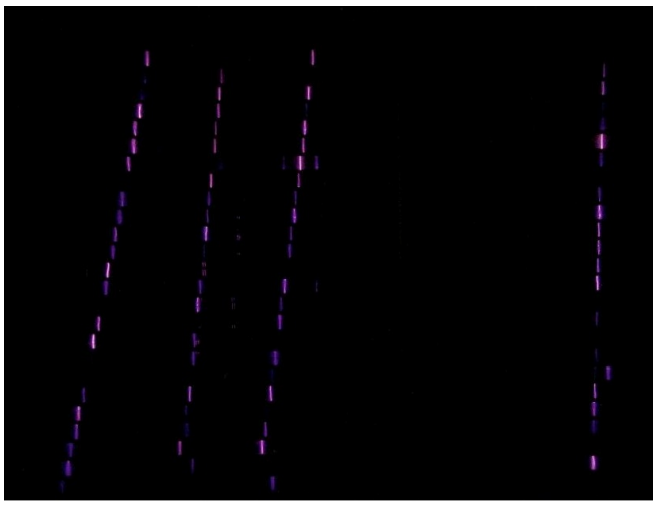

Figure 4: A 30 second exposure of the spark chamber. The image is much clearer than that of figure 3, since it was taken in a much darker environment to hide reflections off the metal plates. A total of 4 trajectories are observed, with small background due to reflections of light off the back Plexiglass border.

The original data analysis procedure (using Matlab) was attempted with figure 4 due to the fact that the particle trajectories are very clear since the metal plates are not seen. Although this image may seem simple, it often happens that 2 or 3 particle trajectories would cross over, in which case it was difficult (even by eye) to tell the difference between the paths. Much progress was made, but the final conclusion was that it would be easier to capture images of single sparks rather than to ask Matlab to separate between the tracks in a dynamic fashion, and analyze them separately. For this reason, a new attempt was made, which is to film the events and analyze the video frame by frame.

Several programs have been written and, when combined, form the visual data acquisition system for the spark chamber. The result is a program that triggers the recording of a video, inputs it to Matlab, and allows each frame to be analyzed. In order to record a good set of data, the room must be completely dark. Therefore, a timer is used to set off the recording system so that there is time to exit the room and ensure that the room is entirely dark. In particular, the program records 10 sets of 1500 frames each and takes approximately one hour to finish recording. It is then possible to return to the room and make sure that the chamber is working properly (specifically that the power supply is still working, refer to section 6) before beginning to record a new set of data.

A typical recorded event can be seen in figure 5.

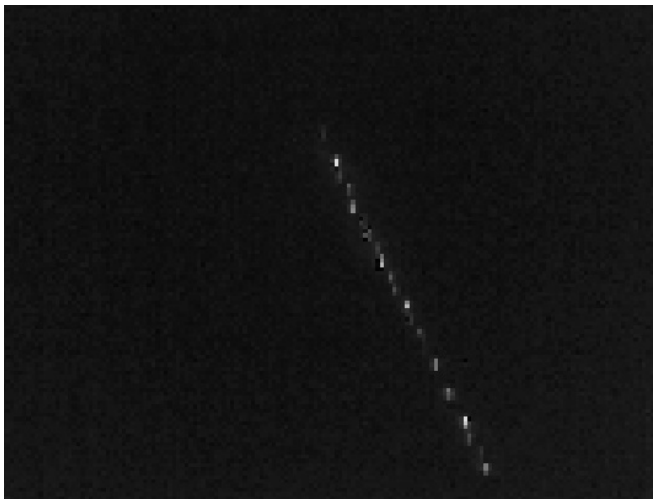

Figure 5: A single event recorded during a video recording using the data acquisition system described above. The event fills exactly one frame of the video recording.

## 5 Data Analysis

Once the frames have been collected, a second program tests each frame to know if a passing particle has been recorded or not. In order to test this part of the program, a frame containing a single event (such as the one seen in figure 5) is selected. The first steps in the data analysis process are to convert the original image to black and white (already completed in figure 5) and to reduce the background noise, which is due to reflections off the back Plexiglass border (see figure 6).

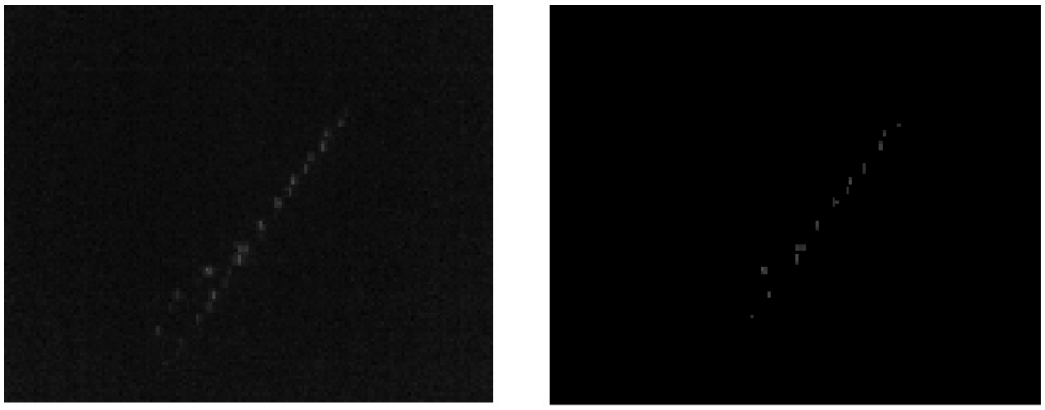


Figure 6: The left image shows a typical event containing background noise after it has been converted to a black and white image. This noise may be due to reflections of sparks off the back wall of the chamber as well as light leaking into the room from outside. The noise is reduced by removing any bright spots that have an intensity lower than a set value. A value of 50 will accomplish this without removing too much of the data since most real sparks have an intensity greater than 80. As can be seen in the cleaned image, the background is erased, while the trajectory of the particle is still present.

The next step is to apply a linear fit to the remaining bright spots. The data may be fit using a linear model because the muons do not curve as they pass through the detector. It is possible to include a magnet in the experiment that will curve the particle's trajectory as it passes through the chamber to know the charge of the muon. In this particular case, it would be necessary to consider a non-linear fit function. However, this is not the case with the spark chamber at McGill, so a linear fit equation may be used.

### 5.1 Linear Fitting

The first fit attempted was a simple linear regression model. This basic fit uses the method of least squares. In general, the resulting fit was appropriate, but if the data contained any outliers, the fit did not follow the data. To account for this, a weight function is introduced and the method of robust linear regression is used instead. In particular, the weight function $w$ is known as the bisquare weight function and is described as:

$$w = \begin{cases} |r| \times (1 - r^2)^2, & if \ \ |r| < 1 \\ 0, & if \ \ |r| \geq 1 \end{cases} \tag{1}$$

The value of $r$ in equation 1 is

$$r = \frac{y - f(x)}{c \cdot s\sqrt{1 - h}},$$

where $y$ is a data point and $f(x)$ is the value of the fit at $y$ so that $y - f(x)$ is a vector of residuals from the previous iteration. $c = 4.685$ is a tuning constant chosen to make the coefficient estimates approximately $95\%$ as efficient as the ordinary least squares estimate, $h$ is a vector of leverage heights from a least squares fit and $s$ is an estimate of the standard deviation of the error.[9] The tuning constants were optimized by Matlab within the fit.

The difference between fitting the data with the ordinary linear regression model and the robust linear

regression model is substantial (see figure 7). The difference in the measured angle of incidence can be as large as 30 degrees in some cases. The reason for this is that the robust regression weighs the points such that any outliers are virtually ignored. Although it is rare to have more than two or three outliers in a single frame, it remains common to have frames with at least one outlier that affects the fit.

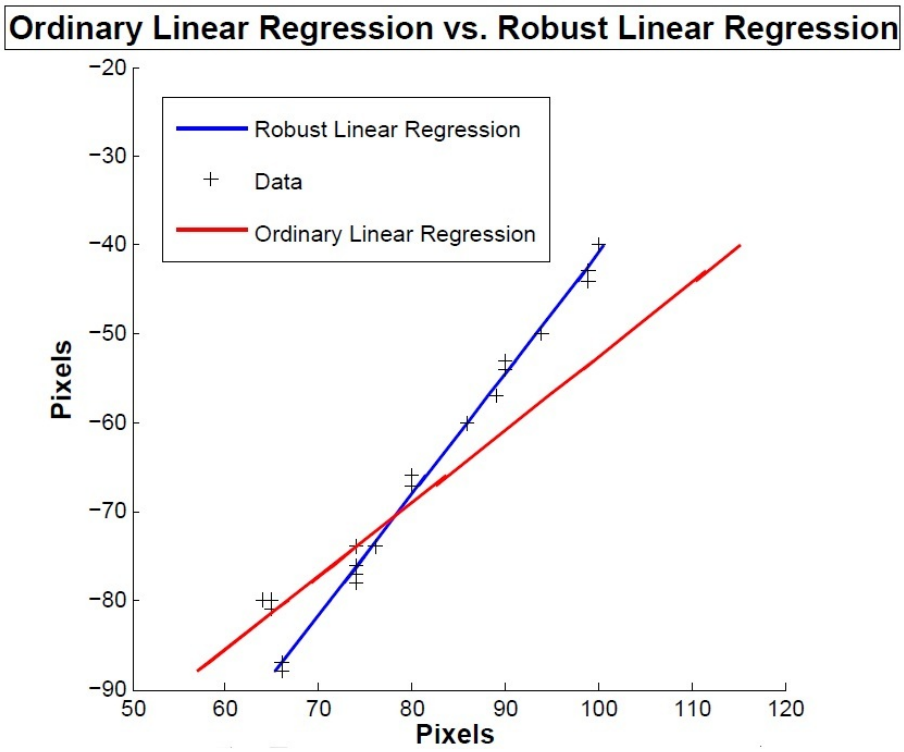


Figure 7: A comparison between the Ordinary Linear Regression model (red) and the Robust Regression Model (blue). The data is shown as black crosses. An outlying spark can be seen in the bottom left corner. This spark is due to a buildup of charge along the plates and does not represent the trajectory of the particle. The Ordinary Linear Regression model weighs all points equally and measures an incident angle of $\theta = 50.5°$ (angles are measured from the vertical). The Robust Linear Regression model, however, weighs each point and essentially neglects outlying points. The fit better represents the data and measures an incident angle of $\theta = 38.5°$, a difference of $12°$.

### 5.2 Selection Criteria

Although the fit is now much better than it was previously, certain tests are in place to decide whether to accept or reject the fit. The first test is a measurement of a value $R^2$, called the Coefficient of Determination.[10] In particular, this value measures to what percent the fit equation predicts the variance in the observed data. For example, a value of $R^2 = 0.89$ says that the fit equation predicts $89\%$ of the variance in the $y$ variable. The $R^2$ value ranges from $0$ to $1$. A value near $0$ says that the fit is not much better than a model of the form $y = constant$ and a value near $1$ means that the fit is good. The cutoff $R^2$ value used in this experiment is $R^2 = 0.9$. This leads to another problem, however, since a particle whose incident angles is at or near $90°$ (meaning a vertical path) will not be accepted even if the fit follows the data perfectly. The reason this happens is that the data will be perfectly linear, so the $R^2$ value will be very low.

The solution is to rotate any image that contains more than a certain number of bright points (approximately 10) higher than the threshold intensity limit of 50 (meaning a particle likely passed through the detector) and has an $R^2$ value less than $0.9$. A rotation of $90^\circ$ will also not work since the trajectory remains straight. Therefore, these images are rotated by $45^\circ$. Once a fit is applied and (if $R^2 > 0.9$) the angle of incidence is measured. The rotation is accounted for by rotating the angle measured back by $45^\circ$.

The second test is one that separates the trajectory of the particle into an upper and lower region and applies a fit to each. The data is accepted if both regions have a fit with a value of $R^2 > 0.9$ *and* the angles measured for each region agree to within $10^\circ$. If both of these conditions are met, then the fit is applied to the entire data set and the angle is measured. The angle is then recorded if it also agrees with the angles measured for each region to within $10^\circ$.

It is now possible to measure the angle of incidence of the particles passing through the detector. Although the final results will be presented with incident angles measured from vertical, the angles measured at this stage are measured from the positive x-axis and are ranged between $0$ and $180^\circ$ to avoid confusion between positive and negative angles in the analysis. The angle $\theta$ is given by $\theta = \tan(m)$, where $m$ is the slope of the fitted line through the data. The angle is later rotated to correspond to the angle of incidence as measured from the vertical and made to range from $-90^\circ$ to $90^\circ$

## 5.3 First Order Corrections

Certain corrections have to be made to do data. The first is to account for the acceptance of the detector and the second is to account for the lack of information in the third dimension. In other words, the trajectories recorded by the camera are not the *true* paths, but are instead the projection of these paths onto the plane parallel to the camera.

### 5.3.1 Acceptance of the Detector

Due to the dimensions of the detector, angles are more likely to be recorded if they are near vertical than if they pass through the detector at an angle away from vertical (see figure 8). A vertical path will be detected by the scintillators at all locations along the detector. In other words, it may pass through any place along the detector of length $L$ and it will be detected. However, a particle entering the chamber at an angle $\theta$ has less of a chance of being detected; it has a smaller surface through which it is detected: $L - \Delta x$.

The acceptance $A$ of the detector is

$$A = \frac{L - \Delta x}{L} = 1 - \frac{h \tan(\theta)}{L}. \tag{2}$$

The dimensions of the detector are:

- L = 62.0 cm
- h = 32.5 cm
- width w = 23.0 cm

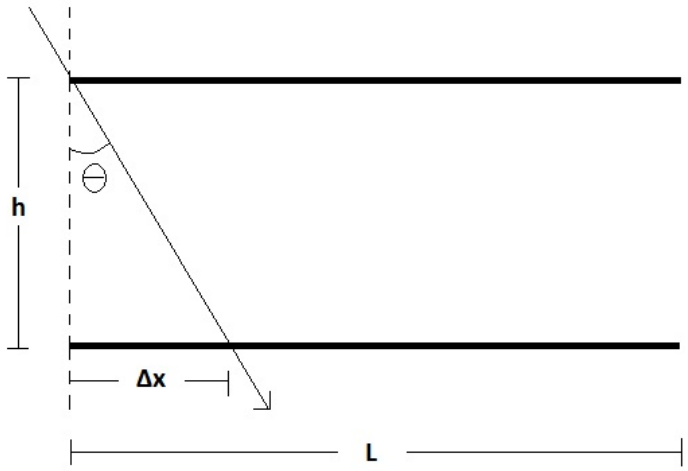


Figure 8: Sketch of the spark chamber detector. $\theta$ is the incident angle of the particle, $h$ is the height of the detector and $L$ is the length. A particle entering the detector at an angle $\theta$ is less likely to be detected by the scintillators than one that enters vertically. In particular, $\Delta x$ is the loss in length along the plate that a particle will be detected by the scintillators.

so the acceptance of the detector is $A = 1 - 0.508\tan(\theta)$. For example, the acceptance of a particle entering the detector at $0^\circ$ from vertical is 1, while $A \to 0$ as $\theta \to 90^\circ$. The data is weighted by dividing by the acceptance.

The maximum incident angle detectable by the scintillators is

$$\theta_{max} = \tan^{-1}\left(\frac{L}{h}\right) = 62.3^\circ \tag{3}$$

#### 5.3.2 Projected Angles

The second correction is less trivial and must account for the fact that the sparks are viewed from one side of the detector only. The ideal solution would be to have two cameras recording simultaneously to produce a 3D reconstruction of the particle trajectories and may be interesting for a future project. However, this project consists of recording the data from one camera only, so the angles recorded are not necessarily the *true* angle of incidence, but are instead the *projected* angle along the plane of the front of the detector. The projection angle $\theta$ may be expressed in term of the true incident angle $\phi$ of the particle (see figure 9 for definitions of $\phi$ and $\alpha$):

$$\theta = \tan^{-1}(\tan(\alpha)cos(\phi)) \tag{4}$$

Since this is the case, the $\cos^2(\phi)$ model does not apply to the angles measured in the experiment, as it predicts the true angle of incidence of the particles (angle $\phi$ in figure 9). The angles $\theta$ measured in this experiment are the projection of the true angles onto a plane. Therefore, a Monte-Carlo sample is created based on the theory that the incoming particles have an angle $\phi$ distributed according to $\cos^2(\phi)$. Since the incoming particles arrive from random directions, the polar angle $\alpha$ is assumed to be distributed according to a uniform random variable between $0^\circ$ and $360^\circ$.

The Monte-Carlo data is designed to represent the distribution of the *projected* angle of incidence.

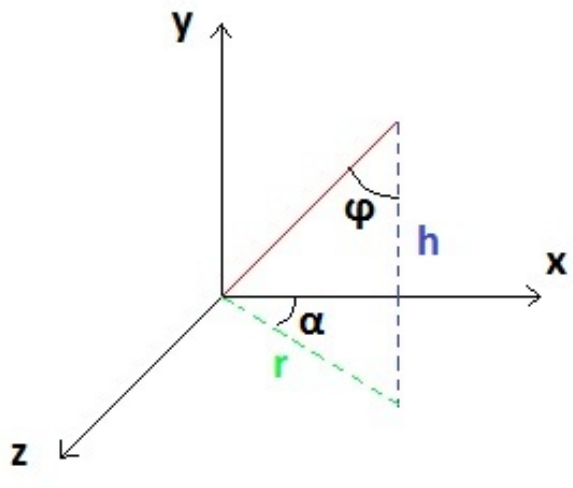


Figure 9: Definition of the angles $\phi$ and $\alpha$ in the Cartesian coordinate system. $\phi$ is the true incident angle of the particle, $\alpha$ is the polar angle, $h$ is the height of the detector and $r$ is the distance between vertical and the spark at heigh $h$.

The data is generated in a pseudo-random fashion by simulating real events (randomly generating angles $\phi$ and $\alpha$ according to their respective distributions), and then projecting these "particles" onto the xy-plane. The distribution of these projected angles is then compared to the collected data. The Monte-Carlo simulation is shown in figure 10.

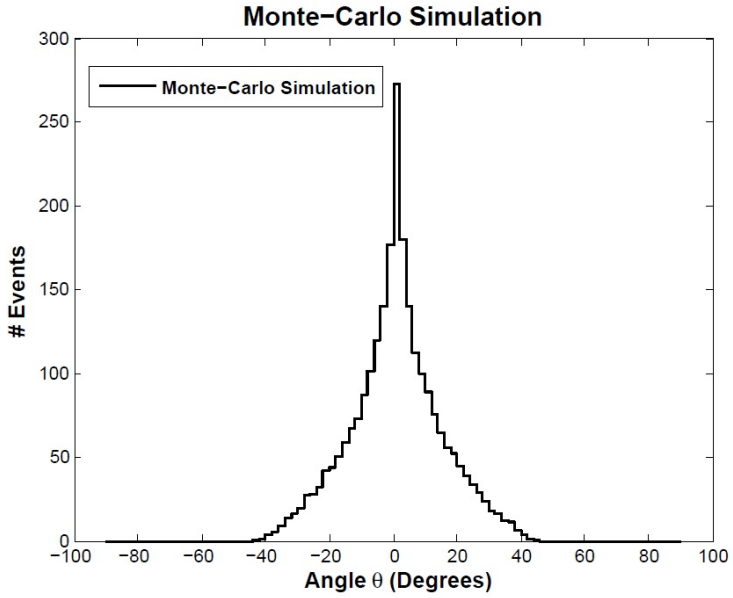


Figure 10: Monte-Carlo simulation of the $\cos^2(\phi)$ distribution after the projection onto the 2D plane.

### 5.4 Error Analysis

In this experiment, the entries within the bins of the histogram are assumed to be governed by Poisson statistics. The reason this is a good assumption is because the Poisson distribution is used when observing the number of events that occur within a certain interval of time and/or space. In this case, we are essentially waiting for the bins of the histogram to be filled with random events. Since the generation of cosmic muons is random in time, the events recorded are independent. Furthermore, this allows us to assume that the mean number of events per bin is the number of entries per bin. For the Poisson distribution, the variance equals the mean. Therefore the error on each bin is simply the square-root of the mean, meaning for a mean $\lambda$, $\sigma = \sqrt{\lambda}$. Since we assumed that $\lambda = \#Entries$, we have $\sigma = \sqrt{\#Entries}$. The entries are later divided by a correction factor (acceptance of the detector) so the errors are also scaled by this factor.

The overall error on the reconstructed angle is approximately $1^\circ$, so the data is binned in intervals of two degrees.

## 6 Results and Discussion

Of the 129 data sets of 1500 frames each, 3191 frames passed the criteria described above and were accepted and analyzed. Although this may seem like a relatively low efficiency for data collection, there are a number of reasons for the low efficiency. In particular, the sensitivity of the power supply to the electromagnetic pickup forced the efficiency to be low since increasing the power caused it to shut down. This effect could be reduced if the chamber were to be set up in a larger room, allowing for a greater distance between the chamber and the power supply. It should also be mentioned that most of the frames are blank frames since there is no triggering mechanism for the camera, and data had to be taken continuously. However, enough time was dedicated to data collection that a large number of events were recorded anyway.

The measured incident angles are placed in a histogram and, as described in the analysis section, the data is adjusted to account for the acceptance of the detector. The result can be seen in figure 11. Theoretically, the peak should be at $0^\circ$ (vertical) and the distribution should be symmetric about zero. It is interesting to note that the peak appears to be shifted towards the left (negative angles). The data is shown alongside the Monte-Carlo simulation where the amplitude of the simulation is chosen to follow the positive angles in the data (see figure 12).

It is clear that the positive end follows the simulation, while the negative end overshoots it. It is also interesting to note that it follows the simulation right before the zero angle. Although many explanations exist to account for this behavior, such as the orientation of the detector with respect to the magnetic field of the Earth, a more likely explanation is a reduction in the efficiency of the scintillators on one end relative to the other. This effect is also seen in figure 13, where the amplitude of the Monte-Carlo simulation is now increased to match the negative angles.

As seen in figures 12 and 13, the measured angles follow the Monte-Carlo data near the end with positive angles, and follow less towards the end with negative angles. In fact, it appears that the data overshoots the model more and more as you move towards the negative end. A likely explanation is that the scintillators may be damaged and trigger more often when a particle passes near the readout

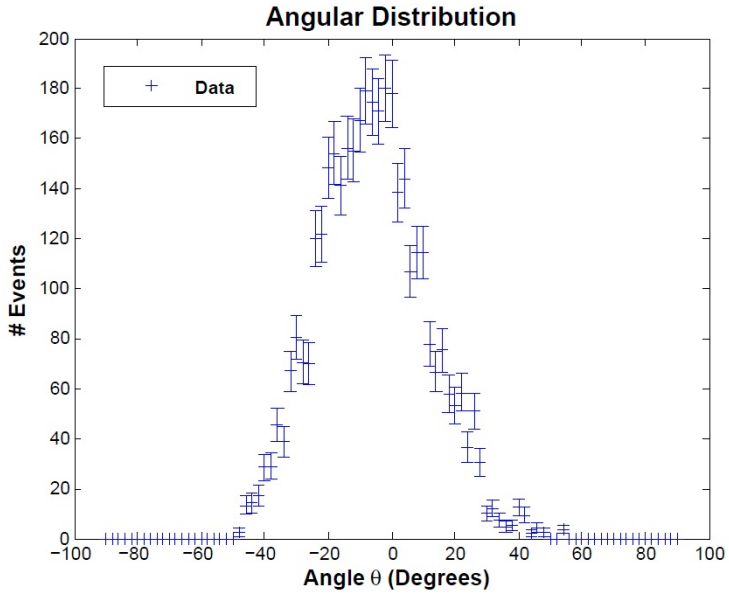


Figure 11: Angular distribution of cosmic muons. Data has been adjusted to account for the acceptance of the detector. The angles are the true angles of incidence projected onto a 2D plane, as seen from the camera recording the sparks.The bin width is $2^\circ$ and error estimates are based on Poisson Statistics and are $\sqrt{\#Events}$ per bin.

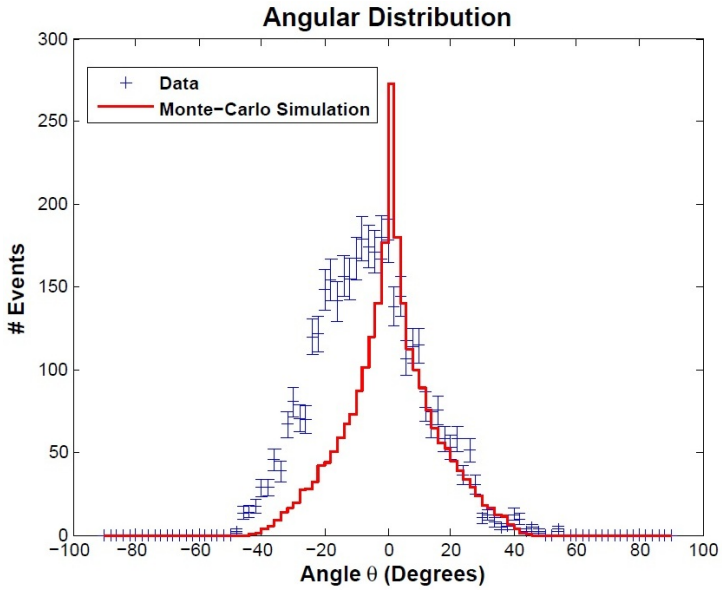


Figure 12: Angular distribution of cosmic muons shown alongside the Monte-Carlo simulation. The amplitude of the Monte-Carlo simulation is chosen so that the shape of the simulation may be compared to the positive angles. The positive angles follows the simulation, while the negative ones overshoot it.

side, into photomultiplier tube. In fact, the setup of the experiment agrees with this explanation since the photomultiplier tubes was oriented towards the left end of the detector throughout the experiment. As seen in figure 13, this effect is even more pronounced as the data undershoots the model near $\theta = 0^\circ$ and overshoots it as $\theta \to -90^\circ$.

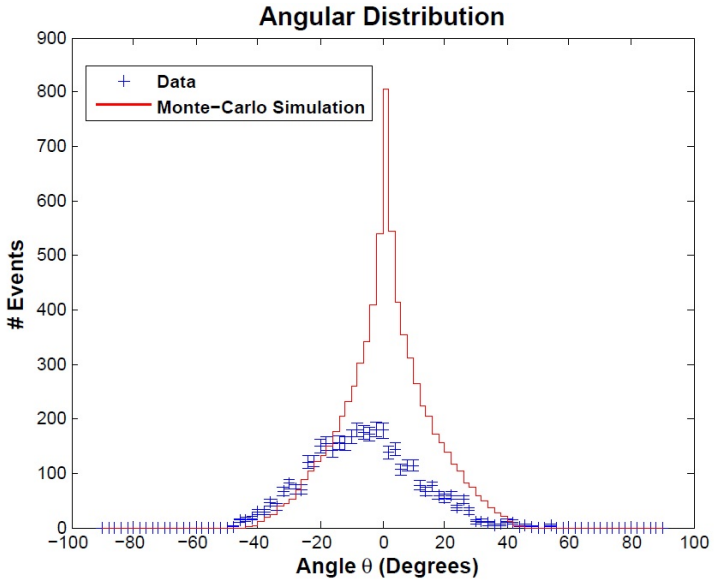


Figure 13: Angular distribution of cosmic muons shown alongside the Monte-Carlo simulation. The amplitude of the Monte-Carlo simulation is chosen to compare the negative end of the data to the simulation. The negative end undershoots the simulation near $\theta = 0°$ and overshoots it as $\theta \to -90°$.

Although the data does not follow the model perfectly, the distribution of the data follows the shape of the model if the data is evaluated at different regions separately. This suggests that an issue occurred, likely to be an issue with the scintillators, that caused the efficiency to vary across the detector. Although tests were done at the beginning of the experiment to make sure the scintillators worked, they were tested as a whole and not as individual parts.

# 7 Conclusion

Many steps have been taken towards building and maintaining a spark chamber at McGill. The goal of this project was to get the chamber working as it used to, while taking the data analysis a step further. During this project, new data acquisition and data analysis software was written. These programs may now be used in future experiments with the spark chamber.

The analysis in this experiment consisted of measuring the angular distribution of cosmic muons and comparing the results to currently accepted models. Although it was not possible to confirm the $\cos^2(\phi)$ model, the data offers no evidence in contrary. However, several structural limitations within the experiment affected the results. Therefore the next step before conducting any more experiments with the spark chamber should be to test the efficiency of the scintillators at every location along their length. The scintillators were tested before the experiment began, but were tested as a whole and not as individual sections.

Future projects already in motion involving the spark chamber at McGill are to improve an acoustic data acquisition method that was previously set up by another summer student. This project is already set to begin and the electronics have already been ordered and received. Another interesting project, which has not yet been suggested, would be to measure the flux of positive and negative cosmic muons by introducing a magnet into the experiment that would curve the muons according to their

charge. The angular distribution of the muons may then be measured for each type.

## 8 Acknowledgments

I would like to thank Prof. F. Corriveau for taking me on for this project and James Kennedy (PhD student for Matt Dobbs) for his time and help with the project. I would also like to thank Sheir Yarkoni for his help and advice on data analysis techniques.

# A Spark Chamber Equipment

### Spark Chamber

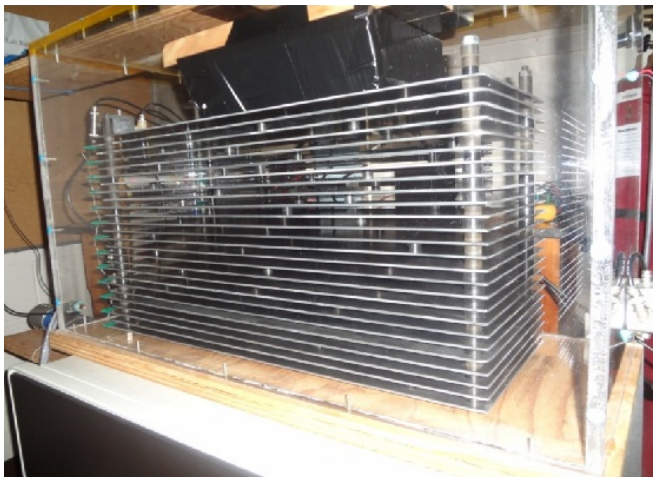

Figure 14: Side view of the spark chamber, currently located in the basement of the Rutherford Physics building at McGill University. The 26 metal plates may be seen here, separated by equally sized rubber stubs and help down by a weight to keep the plates from bending. The plates are enclosed withing a Plexiglass case.

### Scintillators, waveguides and photomultiplier tubes

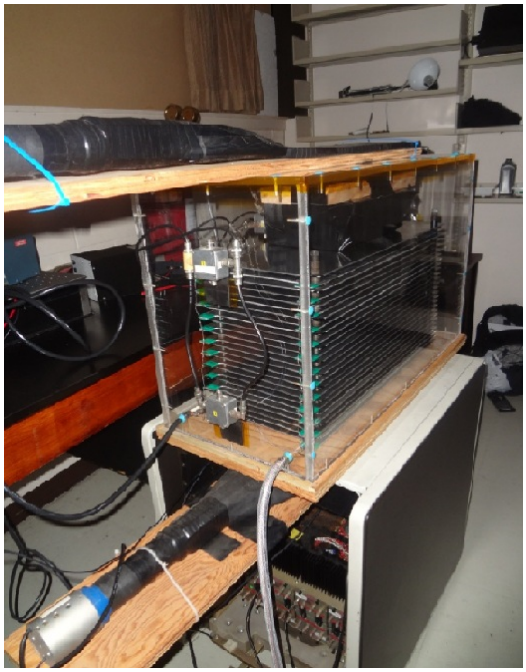

Figure 15: The spark chamber is seen here with the scintillators, waveguides and photomultiplier tubes placed one on top of the detector and one on bottom.

### Piezzo-electric Sensors

Figure 16: Two of the six piezzo-electric sensors may be seen on one edge of the detector. Also, the tube through which helium enters the chamber is seen on the top right of the chamber.

## Electronics

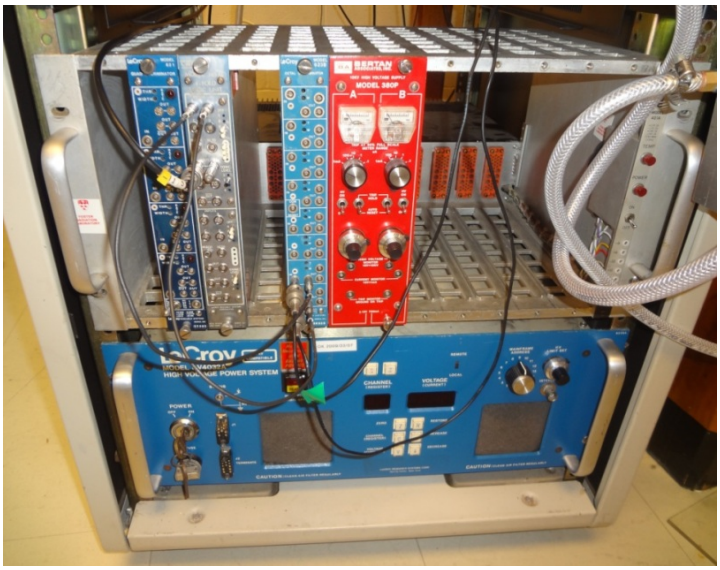

Figure 17: The electronics system. The two power supplies here are the blue and red units. The bottom power supply powers the photomultiplier tubes, while the red power supply powers the spark gap. Also, the discriminator and logic unit can be seen.

## Spark Gap and Spark Gap Circuit Diagram

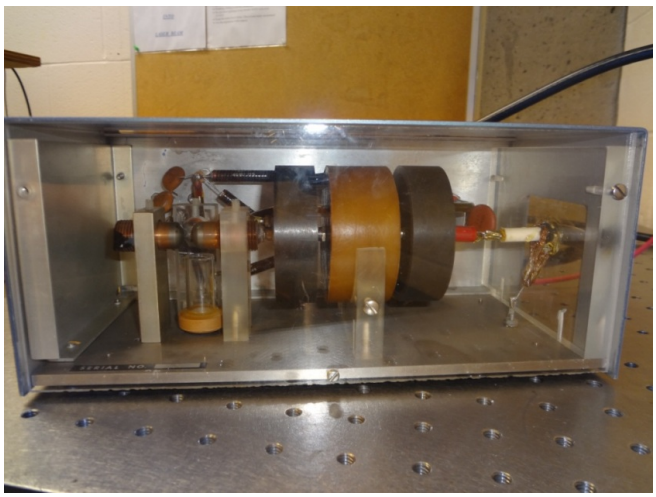

Figure 18: Spark gap

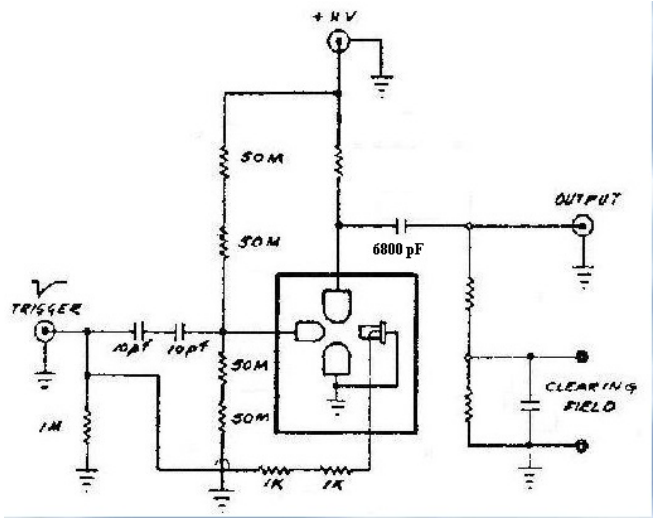


Figure 19: Spark gap diagram

## References


[1] J.W.Keuffel:"Parallel-plate Counters,"Rev.Sci.Instr.20,202-208(1949)

[2] $http://www.australianclimatemadness.com/wp-content/uploads/2011/01/cosmic_ray_shower.jpg$

[3] J.Bernstein, P.Fishbane, S. Gasiorowicz, *Modern Physics*, 71-72

[4] Cosmic Rays, revised August 2011 by J.J Beatty and J. Matthews, $http://pdg.lbl.gov/2011/reviews/rpp2011-rev-cosmic-rays.pdf$

[5] Measuring the Angular Distribution of Muons, Inna Shteinbuk, $http://www.s.u-tokyo.ac.jp/en/utrip/archive/2011/pdf/17Inna.pdf$

[6] T.E. Cranshaw and J.F. DeBeer:"A Triggered Spark Counter," Nuovo Cimento 5, 1107-1116(1957)

[7] Anne-Elisabeth Granier, *Developpement et Construction d'une chambre a etincelles*,McGill University,Juin-Jully 1996,

[8] Michel Pioro-Ladrire, *Computing muon trajectories through the acoustic spark chamber*, McGill University, Apr. 2002

[9] The MathWorks Inc., robustfit, $http://www.mathworks.com/help/toolbox/stats/robustfit.html$

[10] The MathWorks Inc., Derive $R^2$, the Coefficient of Determination, $http://www.mathworks.com/help/techdoc/data_analysis/f1-15377.html\#bswij4t$

[11] Claus Grupen, Boris Shwartz, *Particle Detectors*.Second Edition.

[12] Melissinos A C, *Experiments in Modern Physics*,New York: McGraw-Hill,1966.